Monthly Notices
of the
ROYAL ASTRONOMICAL SOCIETY

Mon. Not. R. Astron. Soc. **426,** 3260–3270 (2012) doi:10.1111/j.1365-2966.2012.21746.x

Excursion set theory for modified gravity: correlated steps, mass functions and halo bias

Tsz Yan Lam[1]★ and Baojiu Li[1,2]★

[1]*Kavli-IPMU, University of Tokyo, Kashiwa, Chiba 277-8583, Japan*
[2]*Institute for Computational Cosmology, Department of Physics, Durham University, South Road, Durham DH1 3LE*

Accepted 2012 July 18. Received 2012 June 11; in original form 2012 May 8

ABSTRACT

We show how correlated steps introduces significant contributions to the modification of the halo mass function in modified gravity models, taking the chameleon models as an example, in the framework of the excursion set approach. This correction applies to both the Lagrangian and Eulerian environments discussed in previous studies. Correlated steps also enhances the modifications arising from the fifth force in the conditional mass function as well as the halo bias. We found that abundance and clustering measurements from different environments can provide strong constraints on the chameleon models.

Key words: large-scale structure of Universe.

1 INTRODUCTION

The discovery of the accelerated expansion of the Universe sparked a surge of research in the possibility of modified gravity models (see, for example, Jain & Khoury 2010; Clifton et al. 2012, for review). The main goal of such modification is to alter the large-scale behaviour to explain the weakening of gravity; however, the modified gravity models must satisfy the tight constraints from the Solar system test. One way to fulfil this requirement is to include some kind of screening mechanism to suppress the modification in the local environment (high-density regime). In this work we focus on one particular example – one that modifies gravity by introducing a dynamical scale field that mediates a fifth force. This scalar field has the nice property that the fifth force is strongly suppressed in regions of high matter density, and hence it passes the Solar system test.

The chameleon model of Khoury & Weltman (2004); Mota & Shaw (2007) is a representative example [other notable examples are the environmentally dependent dilation (Brax et al. 2010) and symmetron (Hinterbichler & Khoury 2010) models]. The background evolution and the linear perturbations on a large scale can be indistinguishable from the standard ΛCDM cosmology (Hu & Sawicki 2007; Li & Barrow 2007; Brax et al. 2008; Li & Zhao 2009); the Solar system test is satisfied by construction. Hence non-linear structure formation is the only regime where the effects of such models would possibly be detected. A number of studies (Oyaizu 2008; Oyaizu, Lima & Hu 2008; Schmidt et al. 2009; Li & Zhao 2009, 2010; Li & Barrow 2011; Zhao, Li & Koyama 2011; Brax et al. 2011; Davis et al. 2012; Li et al. 2012a) employed *N*-body numerical simulations to study non-linear structure formation; however, high-resolution simulations with cosmological volume are still challenging owing to the non-linear equation governing the scalar field.

This work aims to investigate the effect of the chameleon mechanism on large-scale structure. We apply the excursion set approach (Bond et al. 1991; Mo & White 1996; Sheth & Tormen 1999) to compute the halo mass function along the same lines as in previous analyses carried out by Li & Efstathiou (2012) and Li & Lam (2012). Li & Efstathiou (2012) were the first to illustrate the idea of extending the excursion set approach to calculate the halo mass function in chameleon models (see Brax, Rosenfeld & Sterr 2010 for an earlier work in this direction, in which the authors studied the spherical collapse in chameleon models in detail). They did so by assuming a fixed Lagrangian environment. Li & Lam (2012) improved this approach by introducing a Eulerian environment. This choice avoids the unphysical requirement that all environments have the same mass (which also places an upper limit on the halo mass). The calculation involves two first-crossing distributions, one for the Eulerian environment and the other one for the (modified) halo formation barrier. Both studies compute the effect of the chameleon mechanism assuming uncorrelated steps in the excursion set approach – it is the main focus of the first half of the current work to investigate how correlated steps in the excursion set approach interact with the fifth force and the chameleon mechanism. Recently there has been renewed interests in going beyond the uncorrelated steps excursion set in general relativity (GR)+ΛCDM cosmology to compute the halo/void abundance (Maggiore & Riotto 2010; Paranjape, Lam & Sheth 2012a,b; Musso & Sheth 2012) and the halo bias (Ma et al. 2011; Paranjape & Sheth 2012; Musso & Sheth 2012).

In addition to the unconditional mass function, the excursion set approach establishes the framework to calculate the conditional mass function as well as the halo bias. The latter is of particular importance as it relates observables (distribution of halos) to the underlying matter distribution. Because the mass function in chameleon models depends on the environment density, one may

★E-mail: tszyan.lam@ipmu.jp (TYL); baojiu.li@durham.ac.uk (BL)

expect the conditional mass function (and hence the halo bias) to be modified. The second part of this paper discusses how the conditional mass function as well as the halo bias depend on the chameleon model.

This paper is organized as follows. In Section 2 we briefly review the theoretical model to be considered and summarize its main ingredients. The effect of the chameleon mechanism on the halo mass function within the framework of the excursion set approach is presented in Section 3, which includes an analytical approximation for the correlated steps in Section 3.4. Section 4 discusses the conditional mass function and halo bias in chameleon models, and we show that measurements in underdense environments provide a good test for chameleon signatures. Finally, we conclude in Section 5.

2 THE CHAMELEON THEORY

This section establishes the theoretical framework for investigating the effects of a coupled scalar field(s) in cosmology. We present the relevant general field equations in Section 2.1, and then specify the models analysed in this paper in Section 2.2.

2.1 Cosmology with a coupled scalar field

The equations presented in this subsection can be found in Li & Zhao (2009), Li & Zhao (2010) and Li & Barrow (2011), and are presented here only to make this work self-contained.

We start from a Lagrangian density

$$\mathcal{L} = \frac{1}{2}\left[\frac{R}{\kappa} - \nabla^a\varphi\nabla_a\varphi\right] + V(\varphi) - C(\varphi)\mathcal{L}_{\rm DM} + \mathcal{L}_{\rm S}, \tag{1}$$

where R is the Ricci scalar, $\kappa = 8\pi G$ with G being the gravitational constant, and $\mathcal{L}_{\rm DM}$ and $\mathcal{L}_{\rm S}$ are respectively the Lagrangian densities for dark matter and standard model fields. φ is the scalar field and $V(\varphi)$ its potential; the coupling function $C(\varphi)$ characterizes the coupling between φ and dark matter. Given the functional forms for $V(\varphi)$ and $C(\varphi)$, a coupled scalar field model is then fully specified.

Varying the total action with respect to the metric g_{ab}, we obtain the following expression for the total energy momentum tensor in this model:

$$T_{ab} = \nabla_a\varphi\nabla_b\varphi - g_{ab}\left[\frac{1}{2}\nabla^c\nabla_c\varphi - V(\varphi)\right] + C(\varphi)T^{\rm DM}_{ab} + T^{\rm S}_{ab}, \tag{2}$$

where $T^{\rm DM}_{ab}$ and $T^{\rm S}_{ab}$ are the energy momentum tensors for (uncoupled) dark matter and standard model fields. The existence of the scalar field and its coupling change the form of the energy momentum tensor, leading to potential changes in the background cosmology and structure formation.

The coupling to a scalar field produces a direct interaction (fifth force) between dark matter particles owing to the exchange of scalar quanta. This is best illustrated by the geodesic equation for dark matter particles:

$$\frac{{\rm d}^2\boldsymbol{r}}{{\rm d}t^2} = -\nabla\phi - \frac{C_\varphi(\varphi)}{C(\varphi)}\nabla\varphi, \tag{3}$$

where $\boldsymbol{r}$ is the position vector, t the (physical) time, ϕ the Newtonian potential and ∇ the spatial derivative. $C_\varphi \equiv {\rm d}C/{\rm d}\varphi$. The second term on the right-hand side is the fifth force and only exists for coupled matter species (dark matter in our model). The fifth force also changes the clustering properties of the dark matter.

To solve the above two equations we need to know both the time evolution and the spatial distribution of φ; that is, we need the solutions to the scalar field equation of motion (EOM):

$$\nabla^a\nabla_a\varphi + \frac{{\rm dV}(\varphi)}{{\rm d}\varphi} + \rho_{\rm DM}\frac{{\rm dC}(\varphi)}{{\rm d}\varphi} = 0, \tag{4}$$

or equivalently

$$\nabla^a\nabla_a\varphi + \frac{{\rm dV_{eff}}(\varphi)}{{\rm d}\varphi} = 0, \tag{5}$$

where we have defined

$$V_{\rm eff}(\varphi) = V(\varphi) + \rho_{\rm DM}C(\varphi). \tag{6}$$

The background evolution of φ can be solved easily given the present-day value of $\rho_{\rm DM}$ because $\rho_{\rm DM} \propto a^{-3}$. We can then divide φ into two parts, namely $\varphi = \bar{\varphi} + \delta\varphi$, where $\bar{\varphi}$ is the background value and $\delta\varphi$ is its (not necessarily small nor linear) perturbation, and subtract the background part of the scalar field equation of motion from the full equation to obtain the equation of motion for $\delta\varphi$. In the quasi-static limit in which we can neglect time derivatives of $\delta\varphi$ as compared with its spatial derivatives (which turns out to be a good approximation on galactic and cluster scales), we find

$$\nabla^2\varphi = \frac{{\rm dC}(\varphi)}{{\rm d}\varphi}\rho_{\rm DM} - \frac{{\rm dC}(\bar{\varphi})}{{\rm d}\bar{\varphi}}\bar{\rho}_{\rm DM} + \frac{{\rm dV}(\varphi)}{{\rm d}\varphi} - \frac{{\rm dV}(\bar{\varphi})}{{\rm d}\bar{\varphi}}, \tag{7}$$

where $\bar{\rho}_{\rm DM}$ is the background dark matter density.

The computation of the scalar field φ using the above equation then completes the computation of the source term for the Poisson equation:

$$\nabla^2\phi = \frac{\kappa}{2}\left[\rho_{\rm tot} + 3p_{\rm tot}\right] = \frac{\kappa}{2}\left[C(\varphi)\rho_{\rm DM} + \rho_{\rm B} - 2V(\varphi)\right], \tag{8}$$

where $\rho_{\rm B}$ is the baryon density (we have neglected the kinetic energy of the scalar field because it is always very small for the model studied here).

2.2 Specification of model

As mentioned above, to fully fix a model we need to specify the functional forms of $V(\varphi)$ and $C(\varphi)$. Here we will use the models investigated by Li & Zhao (2009), Li & Zhao (2010) and Li (2011), with

$$C(\varphi) = \exp(\gamma\sqrt{\kappa}\varphi) \tag{9}$$

and

$$V(\varphi) = \frac{\Lambda}{\left[1 - \exp\left(-\sqrt{\kappa}\varphi\right)\right]^\alpha}. \tag{10}$$

In the above, Λ is a parameter of mass dimension four and is of the order of the present dark energy density (φ plays the role of dark energy in the models). γ and α are dimensionless parameters controlling the strength of the coupling and the steepness of the potentials respectively.

We choose $\alpha \ll 1$ and $\gamma > 0$ as in Li & Zhao (2009, 2010), ensuring that $V_{\rm eff}$ has a global minimum close to $\varphi = 0$ and that ${\rm d}^2V_{\rm eff}(\varphi)/{\rm d}\varphi^2 \equiv m_\varphi^2$ at this minimum is very large in high-density regions. There are two consequences of these choices of model parameters: (i) φ is trapped close to zero throughout cosmic history so that $V(\varphi) \sim \Lambda$ behaves as a cosmological constant; (ii) the fifth force is strongly suppressed in high-density regions where φ acquires a large mass, $m_\varphi^2 \gg H^2$ (H is the Hubble expansion rate), and thus the fifth force cannot propagate far. The suppression of the

fifth force is even stronger at early times, and thus its influence on structure formation occurs mainly at late times. The environment-dependent behaviour of the scalar field was first investigated by Khoury & Weltman (2004) and Mota & Shaw (2007), and is often referred to as the 'chameleon effect'.

3 FIRST-CROSSING PROBABILITY WITH CORRELATED STEPS IN CHAMELEON MODELS

3.1 Terminology

In the excursion set approach, the calculation of the halo mass function $\mathrm{d}n/\mathrm{d}m$ is mapped to the first-crossing distribution $f(S)$ across some prescribed barrier where

$$\frac{m}{\bar{\rho}}\frac{\mathrm{d}n}{\mathrm{d}m}\mathrm{d}m = f(S)\,\mathrm{d}S. \tag{11}$$

In the following we use the two terms interchangeably. The variance of the matter fluctuation field smoothed on scale R is given by

$$S = \int \frac{\mathrm{d}k}{k}\frac{k^3P(k)}{2\pi^2}W^2(kR), \tag{12}$$

where W is the smoothing window function and $P(k)$ is the matter power spectrum linearly extrapolated to the present time. In hierarchical models S is a monotonic decreasing function of R, and the smoothing scale in Lagrangian space R, the total mass enclosed within this scale M, and the variance S are equivalent quantities and can be used interchangeably.

3.2 Background

Recent work (Li & Efstathiou 2012; Li & Lam 2012) has demonstrated how the chameleon-type fifth force modifies the first-crossing probability and the associated halo mass function for Lagrangian and Eulerian environments. This modification is a result of the dependence of the halo formation barrier height $\delta_c(S)$ on the matter density of its surrounding environment, $\delta_{\rm env}$[1]. Because the fifth force is strongest when the environment density is low, the barrier for halo formation is lower where $\delta_{\rm env}$ is small. The upper panel in Fig. 1 shows the halo formation barrier as a function of S for various values of $\delta_{\rm env}$ assuming that the spherical collapse model describes halo formation, and confirms that the fifth force is stronger in underdense environments where the associated barrier is lower. The actual height that the random walks with various $\delta_{\rm env}$ need to climb to reach the modified barrier is shown in the lower panel – although the barrier in the underdense environment is lower, the barrier to overcome is actually higher.

Li & Efstathiou (2012) and Li & Lam (2012), when applying the excursion set approach in chameleon models, focused on the case in which the excursion set is performed with uncorrelated steps with two different definitions of environment. In both cases the modifications in the first-crossing distribution in chameleon models are solely the result of the change in the barrier. The situation is more complicated when the steps in the random walk are correlated: two additional effects can modify the first-crossing distribution. First, the distribution of $\delta_{\rm env}$ for Eulerian environments is modified, and, because the halo formation barrier depends on $\delta_{\rm env}$, the first crossing probability will be modified as well. Note, however, that when the environment is defined as Lagrangian, the distribution of $\delta_{\rm env}$ is unchanged. Second, there will be non-trivial correlations between the environment density contrast $\delta_{\rm env}$ and the density contrast δ at different S.

[1] Note that in this paper we use $\delta_{\rm env}$ to denote the initial density perturbation in the environment linearly extrapolated to today assuming a ΛCDM model. Knowing $\delta_{\rm env}$, it is straightforward to calculate the true environment density at subsequent times using the assumed evolution model.

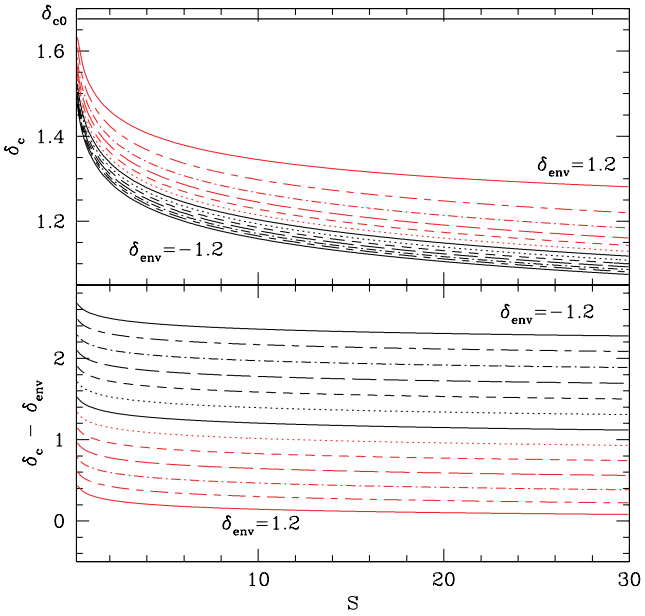

Figure 1. Upper panel: halo formation barrier for various $\delta_{\rm env}$ from −1.2 to 1.2 in increments of 0.2. The constant barrier at the top is the case with no fifth force (i.e. ΛCDM). Lower panel: height needed to be climbed to reach the halo formation barrier for various $\delta_{\rm env}$.

To investigate how these two effects modify the first-crossing distribution in models with the chameleon mechanism, we use Monte Carlo simulations to study the first-crossing distribution for three choices of smoothing window functions following the procedures in Bond et al. (1991). Our convention is such that the normalization of the power spectrum is set by demanding $\sigma_8 = 0.81$ for the tophat filter. The sharp-k smoothing window function generates random walks with uncorrelated steps, and it is common practice to use the S–M mapping of the tophat window function to relate the variance and the smoothing scale for the sharp-k smoothing window function. We consider a ΛCDM power spectrum and two environment scales: a Eulerian environment, denoted by ζ, at late times; and a Lagrangian environment, denoted by ξ, for the initial conditions. We assume that both environments are spherical regions that share the same centres as the proto-haloes. The actual scale of the environment should be approximately the Compton wavelength of the scalar field at late time. Numerical simulation results suggest that a Eulerian scale of $\zeta = 5 \sim 8\,h^{-1}$ Mpc should be chosen (Li, Zhao & Koyama 2012b). In this work we consider a Eulerian environment with $\zeta = 5\,h^{-1}$ Mpc and a Lagrangian environment with $\xi = 8\,h^{-1}$ Mpc, and set $(\gamma, \alpha) = (0.5, 10^{-6})$ as the chameleon model parameters. In the language of excursion set formalism, the Lagrangian environment barrier (fixing S) corresponds to a vertical barrier in the δ_l–S plane, while the Eulerian environment barrier is given by the spherical collapse model (Bernardeau 1994; Sheth 1998):

$$b_{\rm Eul}(S) = \delta_{c0}\left[1 - \left(\frac{M(S)}{\bar{\rho}\zeta}\right)^{-1/\delta_{c0}}\right], \tag{13}$$

where $\bar{\rho}$ is the background density.

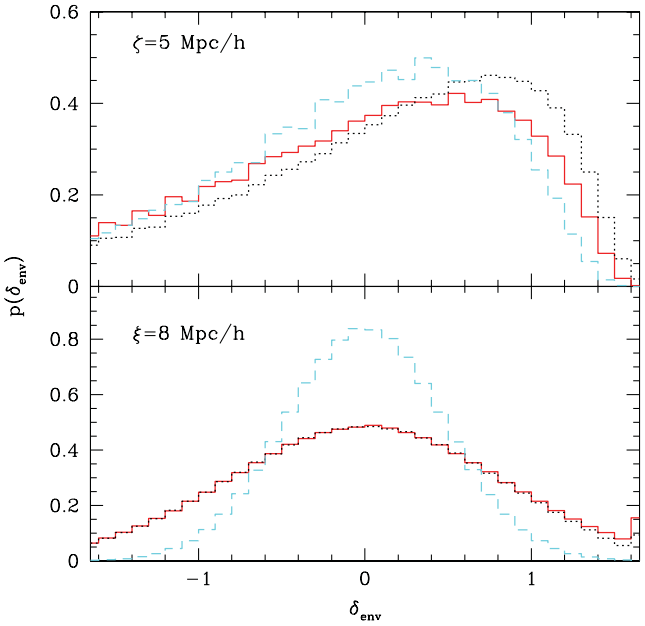

Figure 2. Distribution of environmental density for Eulerian (top panel) and Lagrangian (lower panel) environments. The solid, dashed and dotted curves are the results for tophat, Gaussian and sharp-k window functions respectively.

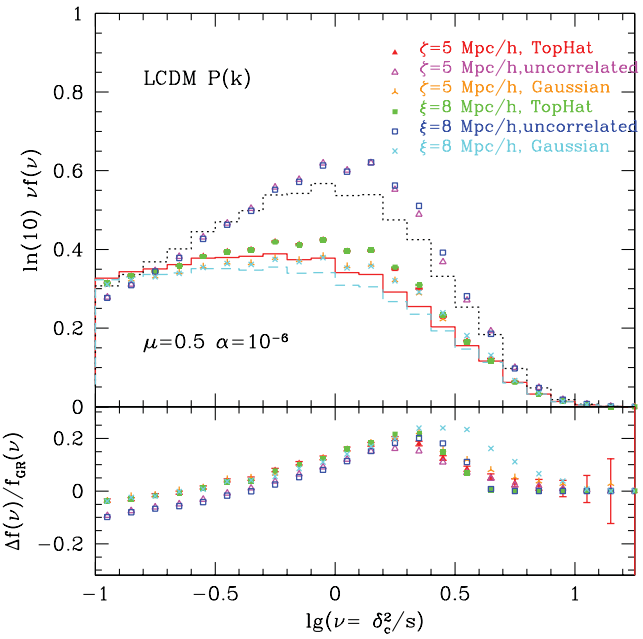

Figure 3. Comparison of the first-crossing distribution in chameleon models for correlated as well as uncorrelated steps. The three sets of histograms are the first-crossing probability for the ΛCDM model with a constant barrier $\delta_c = 1.676$, for different smoothing window functions: (from top to bottom) sharp-k filter (uncorrelated walks), tophat filter and Gaussian filter. The symbols are the first-crossing distribution when there is a fifth force for $\zeta = 5\,h^{-1}$ Mpc and $\xi = 8\,h^{-1}$ Mpc. See legends for details. The bottom panel shows the fractional change in the first-crossing probability with respect to the corresponding constant-barrier first-crossing probability. Only error bars for red solid triangles are included for clarity.

Fig. 2 shows the distribution of $\delta_{\rm env}$ for $\zeta = 5\,{\rm Mpc}\,h^{-1}$ (upper panel) and $\xi = 8\,{\rm Mpc}\,h^{-1}$ (lower panel). Three histograms corresponding to tophat (solid), Gaussian (dashed) and sharp-k (dotted) window functions are shown in each panel. We ran a sample of random walks whose correlation satisfies the corresponding smoothing filter function. We then recorded the height of the random walk at which it first crosses the environmental barrier. In the case of the Lagrangian environment we set $\delta_{\rm env} = \delta_{c0}$ if the random walk first crosses δ_{c0} on a scale bigger than ξ. Because we use the same S–M mapping for the tophat window function and the sharp-k window function, choosing a Lagrangian scale fixes S and hence the two will have the same distribution. The difference between the distributions of Gaussian smoothing and the others in the case of a Lagrangian environment is caused by our choice of power spectrum normalization – for $\xi = 8\,{\rm Mpc}\,h^{-1}$, $\lg(\nu) = 1.1$ for the Gaussian filter, while $\lg(\nu) = 0.62$ for the tophat and sharp-k filters. Here $\nu \equiv \delta_{c0}^2/S$. Because the Lagrangian $\delta_{\rm env}$ distribution is the same for the tophat and sharp-k filters, any difference in their first-crossing distributions resulting from the fifth force has to come from the non-trivial correlations between the height of the random walk and $\delta_{\rm env}$ (see below). On the other hand, the distributions in the Eulerian environment are different for all three smoothing windows: the sharp-k filter peaks at the highest $\delta_{\rm env}$, while the Gaussian filter peaks at the lowest $\delta_{\rm env}$. As a result, the effect of the fifth force is stronger when the Gaussian window function is used – the halo formation barrier for walks with the Gaussian filter is lower than that of uncorrelated walks. Analytical approximations to evaluate the first crossing of the Eulerian environment are available for both uncorrelated (Zhang & Hui 2006; Lam & Sheth 2009) and correlated (Musso & Sheth 2012) steps.

3.3 Monte Carlo simulations

The top panel in Fig. 3 shows the first-crossing distributions in chameleon models for both correlated and uncorrelated walks. The histograms show the distribution when there is no fifth force: it is the first crossing for a constant barrier at $\delta_c = 1.676$. The line labels are the same as in Fig. 2. Symbols represent the first-crossing distributions for different combinations of smoothing window functions and choices of environment, as indicated in the legends. The first-crossing distributions change significantly when the random walks switch from uncorrelated steps (sharp-k) to correlated ones (Gaussian and tophat); using different definitions of the environment has a lesser effect. To better visualize the effect of different choices of the environment, the lower panel shows the relative difference in the distribution from the corresponding constant barrier distribution.

The modifications in the first-crossing distribution arising from the chameleon-type fifth force are quite different for random walks with correlated steps (both Gaussian and tophat filters) than for walks with uncorrelated steps. For example, the modifications of the correlated steps are displaced from those of the uncorrelated steps for $\lg(\nu) < 0.1$. Because the modification in the halo mass function is around 20 per cent, this ∼5 per cent displacement is a big contribution. Consider for example the tophat (solid squares) and the sharp-k (open squares) Lagrangian environments – because they have the same distribution $p(\delta_{\rm env})$, the difference in the predicted modification in the first-crossing distributions must be caused by the non-trivial correlations between the various smoothing scales when the window function is tophat. One can imagine the following scenario: random walks with correlated steps are less likely to have dramatic fluctuations than those with uncorrelated steps – when $\delta_{\rm env} < 0$, the enhanced fifth force lowers the barrier δ_c – in both uncorrelated and correlated cases, it is easier to cross the barrier.

However, correlated walks are not likely to have sudden jumps, and hence the modification in the first crossing comes only at bigger S: it explains the difference between the solid (tophat Lagrangian) and open (sharp-k Lagrangian) symbols for $\lg(\nu) > 0.3$ (the Lagrangian scale $\xi = 8\,\mathrm{Mpc}\,h^{-1}$ corresponds to $\lg(\nu) = 0.62$). For bigger S the correlated walks do not need to have sudden jumps to cross the barrier – hence the increase in the first-crossing probability. On the other hand, the increase for the uncorrelated walks is smaller, as some of those walks already cross the barrier at smaller S. For $\delta_{\rm env} > 0$, the fifth force is weak and only slightly enhances structure formation. In this case walks with correlated steps may cross the barrier sooner than walks with uncorrelated steps (as uncorrelated walks can have a sudden decrease in height). This will result in a higher probability in the first-crossing distribution for correlated steps for S near the chameleon environment; however, this modification in the first-crossing distribution relative to the GR case is small owing to the weakening of the fifth force. Recall that overdense and underdense environments are equally likely in the Lagrangian situation, and the net effect is that correlated steps show a smaller change in first-crossing probability for small s but a bigger change for large s.

The change in the first-crossing distribution for a Gaussian filter and Lagrangian environment is large for high ν. It is consistent with the change in the distribution of $\delta_{\rm env}$ shown in Fig. 2: because $p(\delta_{\rm env})$ has a narrower distribution with a peak at $\delta_{\rm env} = 0$, the overdense environments in the Gaussian case generally have lower $\delta_{\rm env}$, and so the fifth force is stronger (lower barrier) compared with the walks with a tophat or sharp-k filter. On the other hand, the change at the low-mass end is similar to others – although there are more walks that have underdense Lagrangian environments for the other two filters, those walks need to climb a huge distance to cross their respective modified barriers and do not make a significant contribution in the first-crossing distribution.

3.4 Analytical approximation

In this subsection we apply the analytical approximation proposed by Musso & Sheth (2012) to estimate the first-crossing distribution in chameleon models. In this analytical approximation, the first-crossing probability at s is approximated by both the height and its rate of change at $s - \Delta s$. The first-crossing distribution across barrier $b(s)$ [2] is

$$f(s) = p(b, s) \int_{b'}^{\infty} \mathrm{d}\delta'\ p(\delta'|b, s)(\delta' - b'), \tag{14}$$

where the dash denotes the derivative with respect to s, $p(\delta'|b, s)$ is the conditional probability density of the rate of change in height δ' at s given that the walk's height is b at the same scale s, and $p(\delta, s)$ is the probability density that the walk has height b at the smoothing scale s.

When the Lagrangian environment is used in the chameleon models, the first-crossing distribution of the modified barrier $b = \delta_c(s, \delta_{\rm env})$ at s is

$$f_{\rm Lag}(s; \xi) = \int_{-\infty}^{\delta_{c0}} \mathrm{d}\delta_{\rm env}\ p(\delta_{\rm env}, \xi) p(b, s|\delta_{\rm env}, \xi) \times \int_{b'}^{\infty} \mathrm{d}\delta'\ p(\delta'|b, s; \delta_{\rm env}, \xi)(\delta' - b'), \tag{15}$$

[2] In this subsection we use upper and lowercase letters to denote different smoothing scales and random walk heights.

where $p(\delta_{\rm env}, \xi)$ is the distribution of the environmental density contrast at scale ξ. Strictly speaking, $p(\delta_{\rm env}, \xi)$ should be replaced by the conditional probability that δ never crosses δ_{c0} for scales larger than ξ, but the scales we apply to the Lagrangian environment are large enough that the difference between the two is small.

Fig. 4 shows the comparison of the analytical approximation and the Monte Carlo results for the Lagrangian environment of $\xi = 8\mathrm{Mpc}\,h^{-1}$. The upper panel shows the results of a Gaussian window function, while the lower panel shows the tophat window function. In each panel the top half shows the first-crossing distribution from the analytical prediction (curve) and the Monte Carlo result (symbols), and the bottom half shows the modifications to the first-crossing distribution relative to GR. The analytical approximation matches the Monte Carlo simulation for $\lg(\nu) > 0$. For smaller ν, multiple crossings are more frequent and the approximation breaks down.

The first-crossing distribution for a Eulerian environment contains two first crossings: first to cross the environment barrier, and then the halo formation barrier. Applying the approximation to both crossings yields

$$f_{\rm Eul}(s, \zeta) = \int_0^s \mathrm{d}S\ p(B, S) \int_{B'}^{\infty} \mathrm{d}\Delta'\ p(\Delta'|B, S)(\Delta' - B') \times p(b, s|B, S; \Delta') \times \int_{b'}^{\infty} \mathrm{d}\delta'\ p(\delta'|b, s; B, S; \Delta')(\delta' - b'), \tag{16}$$

where we denote the Eulerian environment barrier as $B(S)$ and Δ' is the derivative of $\delta_{\rm env}$ at S. The dependence of the halo barrier $b(s)$

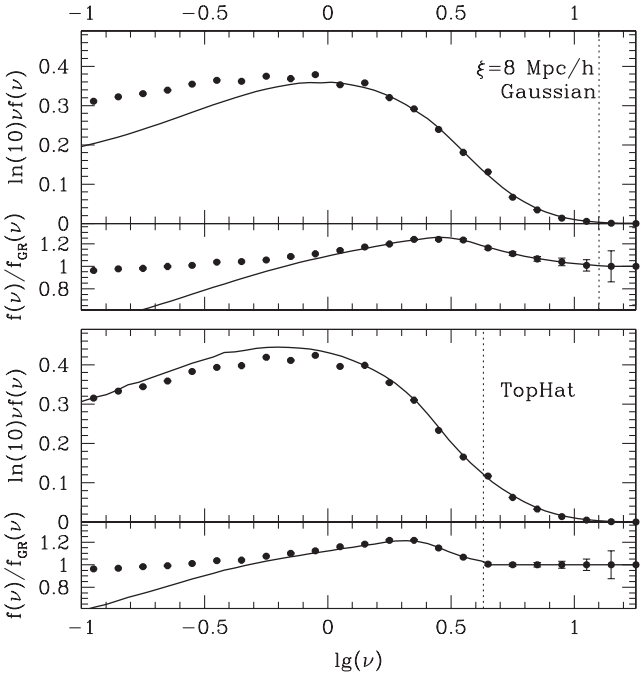

Figure 4. Analytical approximation for the first-crossing distribution in chameleon models for correlated steps. The upper and lower panels show the results using a Lagrangian environment $\xi = 8\,\mathrm{Mpc}\,h^{-1}$ for Gaussian and tophat window filters, respectively. In each figure the curve is the analytical approximation, while the data points are Monte Carlo simulation results. The upper half of each figure shows the first-crossing distribution, and the lower half shows the ratio to the constant-barrier distribution. The vertical dashed lines show the scales of the Lagrangian environment.

on $B(S)$ is implicit. The first integral includes walks with different Eulerian environment density contrasts (up to s), while the second integral corresponds to the first crossing of the Eulerian barrier at S. Here, the upper limit of the integration should have been replaced such that the walk would not cross δ_{c0} at S. In practice, however, the probability of having a big jump is unlikely, so using the above approximation does not alter the result. Finally, the rest corresponds to the first crossing of the modified halo barrier at s given the walk first crossed the Eulerian barrier at S with an increase in height Δ' when going from $S - \Delta S$ to S. The results are shown in Fig. 5. The analytical approximation works relatively well for large ν (>1) but breaks down for small ν, as in the case of the Lagrangian environment.

The conditional probability distributions in this subsection are also Gaussian-distributed with mean and variance given by

$$\mathrm{E}(x|y_1, y_2, \ldots, y_n) = \sum_{i,j=1}^{n} \langle x y_i \rangle A_{ij}^{-1} y_j \tag{17}$$

$$\mathrm{Var}(x|y_1, y_2, \ldots, y_n) = \mathrm{Var}(x) - \sum_{j=1}^{n} \langle x y_j \rangle^2 A_{jj}^{-1} - 2 \sum_{j>k} \langle x y_j \rangle \langle x y_k \rangle A_{jk}^{-1}, \tag{18}$$

where $\mathbf{A}$ is the covariance matrix of $\{y_i\}$ and we assume that all variables have unconditional means that vanish in the above formuale.

4 CONDITIONAL MASS FUNCTION AND HALO BIAS IN CHAMELEON MODELS

In this section we describe the effect of the chameleon-type fifth force on the conditional mass function and the halo bias. As explained in the previous section, the fifth force is stronger when the environment is less dense – effectively the halo formation criterion is lower and hence the first crossing of the halo formation barrier is easier. It may then be asked if this effect will be more significant when we look at the conditional mass function, especially for underdense regions. Here we will use Monte Carlo simulations to investigate how the conditional mass function responds to the fifth force introduced by the chameleon models.

We now have two environments: one is used to solve the fifth force in the chameleon model (we will call it the *chameleon* environment hereafter and we choose $\zeta = 5\,h^{-1}$ Mpc and $\xi = 8\,h^{-1}$ Mpc) and the other is a *large-scale* environment $S = S_0$ on which the condition is defined. We choose S_0 to be small (hence very large scale) so that it is safe to assume that the range of the fifth force is much smaller than the scale corresponding to S_0.

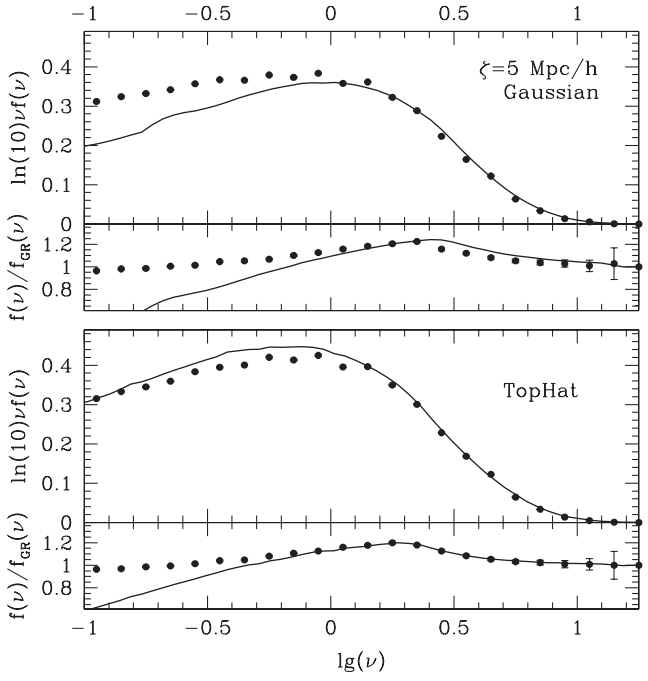

Figure 5. Similar to Fig. 4, but using a Eulerian environment with $\zeta = 5\,\mathrm{Mpc}\,h^{-1}$.

4.1 Conditional first-crossing probability in chameleon models

In this subsection we look at the conditional first-crossing probability for three smoothing window functions. The conditional first-crossing probability is

$$f(S|\delta_0, S_0) = \int \mathrm{d}\delta_{\rm env}\; f(S|\delta_{\rm env}; \delta_0, S_0) P(\delta_{\rm env}|\delta_0, S_0), \tag{19}$$

where $f(S|\delta_{\rm env}; \delta_0, S_0)$ is the conditional first-crossing probability across the $\delta_c(S, \delta_{\rm env})$ barrier given that the random walk in consideration first crosses the environment barrier $B(s)$ at $\delta_{\rm env}$ *and* it has $\delta = \delta_0$ at S_0. $P(\delta_{\rm env}|\delta_0, S_0)$ is the conditional first-crossing probability of crossing the environment barrier at $\delta_{\rm env}$. Changing the large-scale environment can have two effects, as follows.

(i) Changing the large-scale environment modifies the distribution of $\delta_{\rm env}$: when $\delta_0 < 0$, the distribution of the chameleon environment is more likely to have a less dense chameleon environment ($\delta_{\rm env}$ is smaller), and hence the fifth force will be stronger.

(ii) Changing the large-scale environment also affects the first-crossing distribution of the halo formation barrier when the random walk is non-Markovian (this effect is additional to the first point, where the halo formation barrier is changed owing to the change in the environment distribution).

One may expect the second effect to be weaker than the first, as the correlation is weaker for a bigger difference in S. In particular, for the sharp-k filter when the random walks have uncorrelated steps, the walks are Markovian, and the large-scale environment (δ_0, S_0) only modifies the distribution of $\delta_{\rm env}$; that is,

$$f_{\rm uncor}(S|\delta_{\rm env}; \delta_0, S_0) = f(S|\delta_{\rm env}). \tag{20}$$

We quantify the effect in this section using Monte Carlo simulations. We choose two large scales ($S_0 = 0.15^2\delta_{c0}^2$ and $0.25^2\delta_{c0}^2$) and measure the conditional first-crossing distributions using different window filters.

Figs 6 and 7 show the conditional first-crossing distributions for various choices of δ_0 at $S_0 = 0.15^2\delta_c^2$ and $0.25^2\delta_c^2$, respectively. In each panel the histograms indicate the first-crossing probability for the constant barrier case (ΛCDM), while the solid and the open symbols represent chameleon models with $\zeta = 5\,\mathrm{Mpc}\,h^{-1}$ and $\xi = 8\,\mathrm{Mpc}\,h^{-1}$, respectively. Three sets of distribution are included in each panel: conditional probability with $\delta_0 > 0$ (highest-amplitude histogram at $\lg(\nu) = 0.5$ and squares), conditional probability with $\delta_0 < 0$ (lowest-amplitude histogram at $\lg(\nu) = 0.5$ and pentagons), and unconditional probability (the intermediate

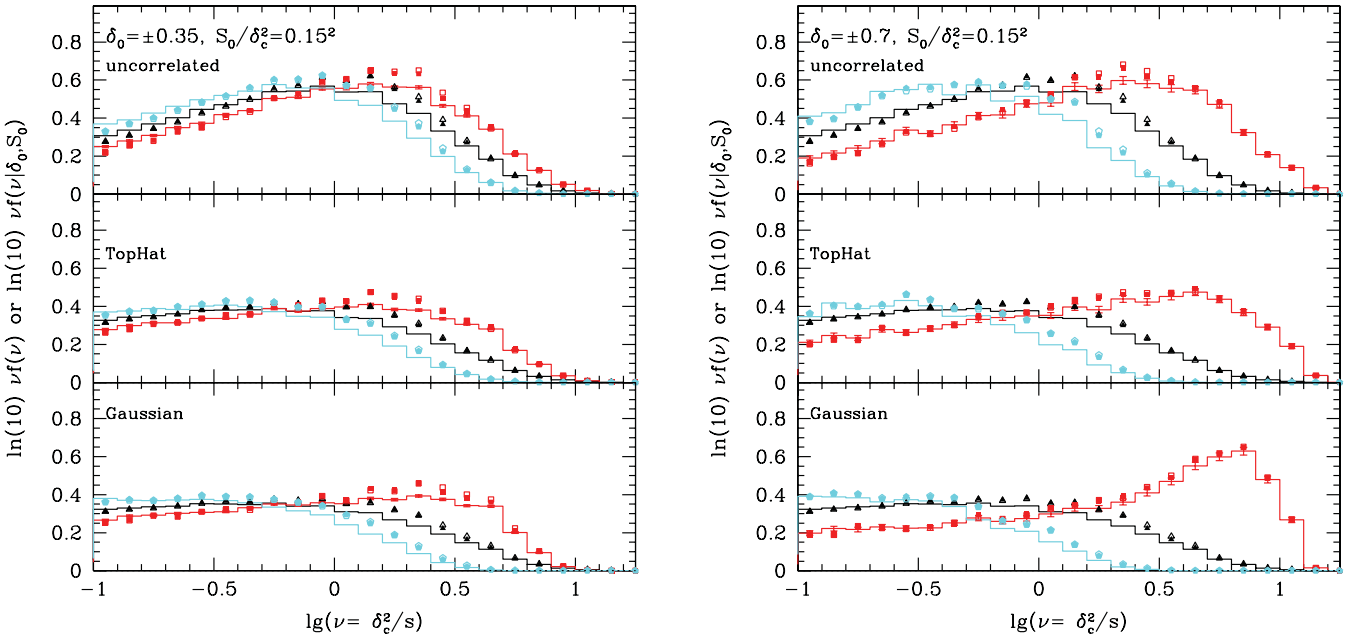

(a) $\delta_0 = \pm 0.35$ (b) $\delta_0 = \pm 0.7$

Figure 6. Comparison of the conditional first-crossing probability obtained from Monte Carlo simulations for uncorrelated and correlated steps by selecting subsets of walks that have various values of δ_0 at $S_0 = 0.15^2\delta_c^2$. In each panel the histograms indicate the first-crossing probability for the constant-barrier case (ΛCDM), while the solid symbols and the open symbols represent chameleon models with $\zeta = 5\,h^{-1}$ Mpc and $\xi = 8\,h^{-1}$ Mpc, respectively. Three sets of probability are included in each panel: $|\delta_0|$ (highest-amplitude histogram at $\lg(\nu) = 0.5$ and squares); $-|\delta_0|$ (lowest-amplitude histogram at $\lg(\nu) = 0.5$ and pentagons); and unconditional probability (the intermediate histogram and triangles). Different panels use different smoothing window functions: (from top to bottom) uncorrelated steps; tophat window function; Gaussian window function. Only error bars for the histogram for positive δ_0 are included for clarity.

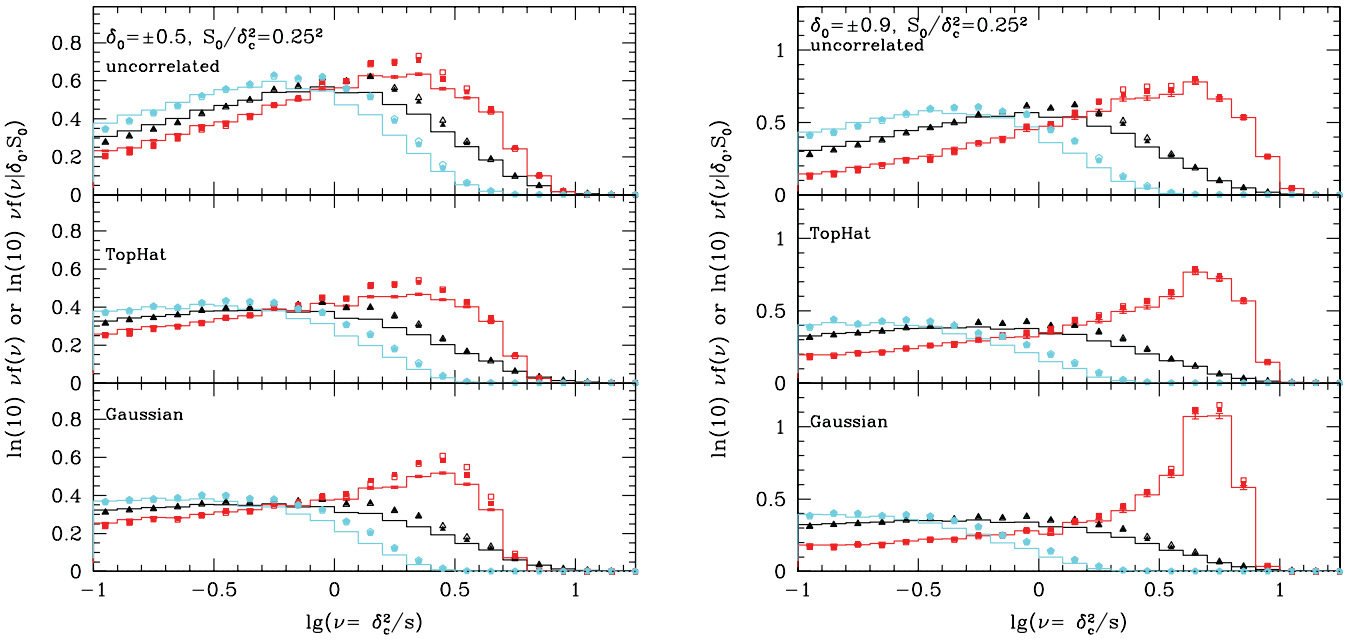

(a) $\delta_0 = \pm 0.5$ (b) $\delta_0 = \pm 0.9$

Figure 7. Conditional first-crossing probability similar to Fig. 6. The condition is set at $S = 0.25^2\delta_c^2$.

histogram and triangles). Different panels use different smoothing window functions – from top to bottom: sharp-k, tophat and Gaussian filters. The conditional mass function differs from the unconditional mass function, and the change depends on the smoothing window function as well as on the large-scale density contrast δ_0: in general, conditional distributions using Gaussian or tophat window functions and having more extreme values of δ_0 show more significant changes than the respective unconditional distributions.

The large-scale environment modifies the distribution of the linear density contrast in the chameleon environment, which in turn modifies the first-crossing distribution. The modification depends on the smoothing window functions owing to the difference in correlation strength between the various scales involved (the large-scale environment, the chameleon environment, as well as the scale at which the halo barrier is first crossed). We took the ratio of the change in the first-crossing distribution for conditional walks to that of the unconditional walks, and the results are shown in Figs 8 and 9 for $\delta_0 = \pm 0.5$ and ± 0.9, respectively, when $S_0 = 0.25^2\delta_{c0}^2$. The upper and lower panels of the two figures show respectively the Eulerian and the Lagrangian environment for the chameleon models. In each panel the ratios for $\delta_0 < 0$ are shifted upwards by 0.1, and symbols represent different smoothing window kernels: open symbols for sharp-k, solid symbols for tophat, and starred symbols for Gaussian.

If the change in the first-crossing probability induced by the chameleon-type fifth force did not depend on the large-scale environment, this ratio should be unity (indicated by the dashed horizontal line). Ratios above (below) unity indicate that those walks

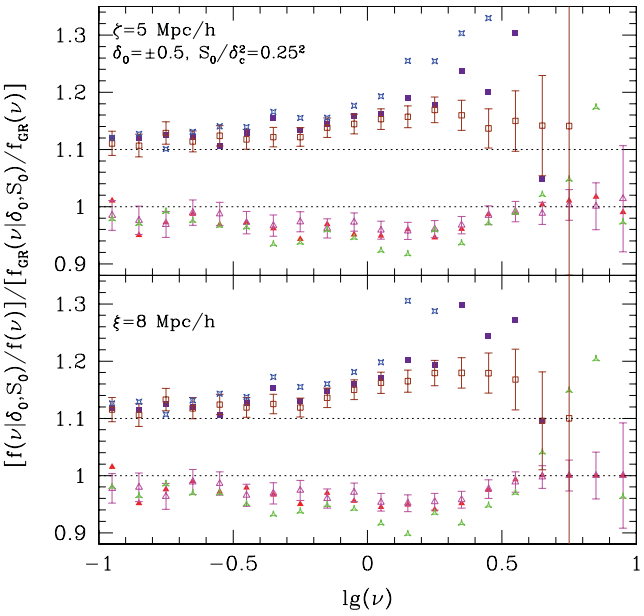

Figure 8. Comparison of how the change in first-crossing probability owing to the fifth force depends on the large-scale environment (δ_0, S_0). The ratios are taken from the conditional distributions of Fig. 7(a) and compared with ratios taken from the unconditional distributions. The upper panel shows results with the Eulerian environment with $\zeta = 5\,\mathrm{Mpc}\,h^{-1}$, and the lower panel is the Lagrangian environment with $\xi = 8\,\mathrm{Mpc}\,h^{-1}$. The two sets of points in each panel indicate $\delta_0 = 0.5$ (lower set) and $\delta_0 = -0.5$ (upper set, shifted by $+0.1$), respectively. Each set has three symbols representing different window functions: open (uncorrelated walks), solid (tophat), starred (Gaussian). Only error bars for uncorrelated walks are included, as an approximate error indicator.

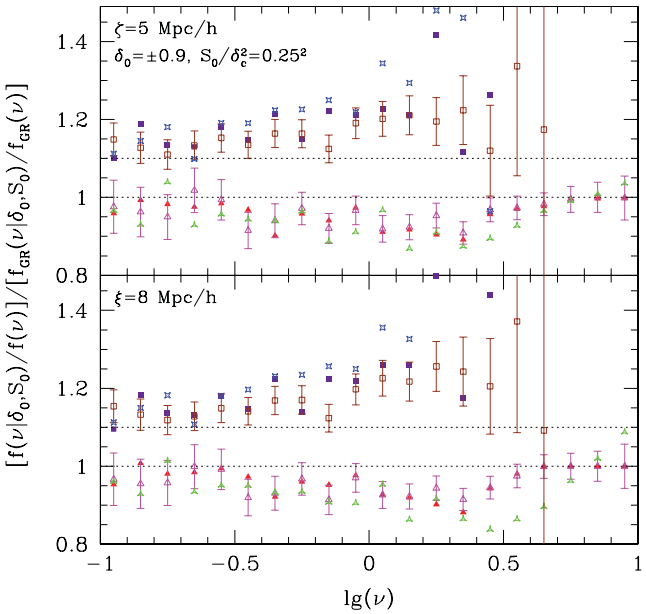

Figure 9. Conditional first-crossing probability similar to Fig. 8 (note the change in y-axis range), but the subsets of walks pass through $\delta_0 = \pm 0.9$.

experience a stronger (weaker) chameleon effect compared with the unconditional walks. They also make relatively bigger (smaller) contributions to the change in the unconditional first-crossing distribution. The Monte Carlo results are consistent with expectations: for walks that have a slightly overdense large-scale environment ($\delta_0 > 0$), the ratio is always less than unity – these walks are more likely to have overdense $\delta_{\rm env}$ (regardless of the choice of Eulerian or Lagrangian environment), and hence the strength of the fifth force is weaker. The ratios for walks with correlated steps (solid and starred triangles) have larger deviations from unity compared with the ratio for walks with uncorrelated steps (open triangles), indicating that the conditional distribution of $\delta_{\rm env}$ has stronger correlations with δ_0 when steps are correlated (otherwise the correlation between δ_0 and δ at some larger s should result in higher probability in first crossing). When the value of δ_0 is more extreme, the deviation from unity is bigger, indicating further weakening of the fifth force.

On the other hand, for walks that have underdense large-scale environments ($\delta_0 < 0$), the ratio for both uncorrelated and correlated walks stays above unity: the change in the first-crossing distribution owing to the fifth force is stronger than that for the unconditional walks. The ratio goes significantly above unity for correlated steps, indicating that the abundance of intermediate-mass haloes in underdense environments would potentially provide a strong constraint on the chameleon-type fifth force.

Fig. 10 shows a similar plot but with the large-scale environment set at $S_0 = 0.15^2\delta_{c0}^2$. A comparison with Fig. 8 indicates that, while the conditional distribution $p(\delta_{\rm env}|\delta_0, S_0)$ still differs from the unconditional distribution $p(\delta_{\rm env})$, the difference is less significant – a very large environment ($S_0 = 0.15^2\delta_{c0}^2$) has weaker correlations with the chameleon environment compared with the previous case where $S_0 = 0.25^2\delta_{c0}^2$.

In this subsection we have studied the conditional mass function in chameleon models. The correlation between the large-scale environment and the chameleon environment induces further modifications in the first-crossing distribution – this effect is strongest (in terms of the modification of the conditional mass function)

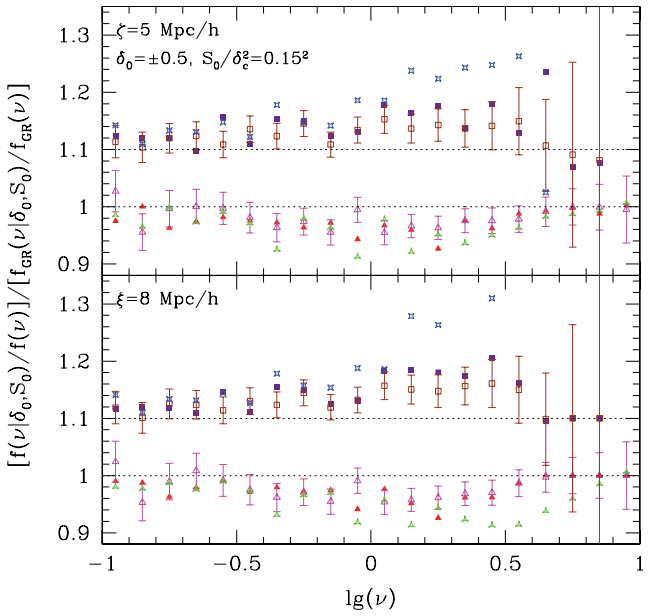

Figure 10. Conditional first-crossing probability similar to Fig. 8, but the subsets of walks pass through $\delta_0 = \pm 0.5$ at $S_0 = 0.15^2\delta_{c0}^2$.

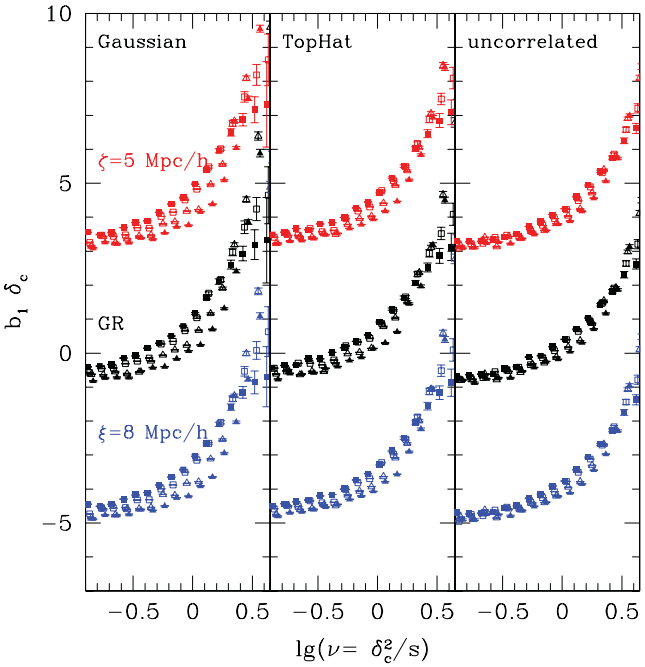

Figure 11. Halo bias computed from Monte Carlo simulations using equation (22). We chose $S_0 = 0.15^2\delta_{c0}^2$ and $\delta_0 = \pm 0.35$ (solid) or ± 0.5 (open) for the conditional first-crossing distribution, where triangles (squares) represent positive (negative) δ_0.

when the large-scale environment is underdense. The corresponding change in the halo mass function for intermediate-mass haloes shows an extra ∼30 per cent boost compared with the unconditional mass function. It is straightforward to extend the analytical approximation in Section 3.4 to obtain the conditional first-crossing distribution by including an additional condition (δ_0, S_0) in all the probability distributions in equations (15) and (16). This is beyond the scope of this work.

4.2 Halo bias in chameleon models

Halo bias describes the relationship between the halo overdensity δ_h and the matter overdensity δ, where the halo overdensity can be expanded as

$$\delta_h = \sum_{i=1} \frac{b_i}{i!}\delta^i. \tag{21}$$

For large scales the above expansion can be truncated in the first few orders. In particular, the linear bias term b_1 is commonly used to fit the ratio between the halo-matter power spectrum $P_{h\delta}$ and the matter power spectrum $P_{\delta\delta}$ (or its square as the ratio between the halo power spectrum P_{hh} and $P_{\delta\delta}$). The excursion set approach provides a natural way to relate halo abundance and halo bias – by starting the random walks at some prescribed locations rather than the origin (Mo & White 1996; Sheth & Tormen 1999). The relative difference of this conditional first-crossing probability from the unconditional one gives the left-hand side of equation (21).

Recently there have been several studies focused on evaluating the halo bias using the excursion set approach with correlated steps, for example Ma et al. (2011) and Paranjape & Sheth (2012). Both of the analyses (using very different methods) found that the halo bias with correlated steps is stronger than that for the uncorrelated case. Paranjape & Sheth (2012) also suggested that, when correlated steps are considered, the halo bias computed from the excursion set approach is different from the one obtained by taking the ratio of the halo-matter power spectrum and the matter power spectrum. While we are interested in computing the halo bias with correlated steps, we do not make the distinction here and we will present the halo bias evaluated within the excursion set framework.

In the chameleon models the halo formation barrier in the excursion set approach depends on the environment density. To estimate the halo bias we use the conditional first-crossing distributions obtained in the previous subsection and compute the halo bias from equation (21), where

$$b_1\delta_{c0} = \left[\frac{f(S|\delta_0, S_0)}{f(S)} - 1\right]\frac{\delta_{c0}}{\delta_0}, \tag{22}$$

assuming that high-order terms can be neglected. We chose the conditional first-crossing distribution where $S_0 = 0.15^2\delta_{c0}^2$ and $\delta_0 = \pm 0.35$ and ± 0.5, and the results are shown in Fig. 11. The three panels show results using different smoothing window functions, and the results for chameleon models are shifted by ± 4.

Halo bias using more strongly correlated window functions has a stronger dependence on the value of δ_0, which can be seen by comparing the spread of bias among the three panels. Inclusion of the chameleon-type fifth force modifies the halo bias, and the relative changes are shown in Figs 12 and 13 for the Eulerian and Lagrangian environments respectively. In both environment definitions the relative difference of the halo bias in chameleon models can be a factor of a few, regardless of the window function used. Another noticeable signature is the difference of the mass range where the halo bias relative difference is most significant: when tophat or Gaussian window filters are used, the change in halo bias for the most overdense environment (triangles, $\delta_0 = 0.5$) is most significant around $\lg(\nu) = -0.1$, but it is shifted to lower masses $\lg(\nu) = -0.5$ for underdense environments (solid lines, $\delta_0 = -0.5$). This difference in mass range becomes smaller when δ_0 is less extreme (see the difference between the squares and dotted lines for

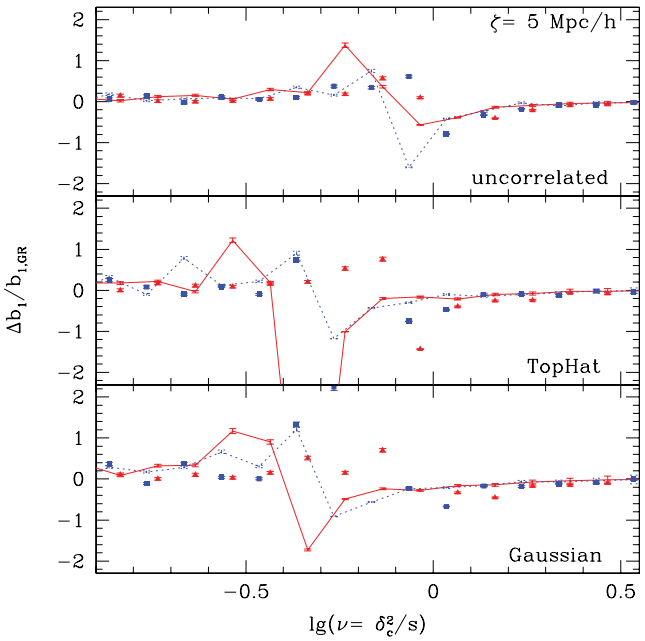

Figure 12. Relative difference in halo bias for chameleon models (Eulerian environment) from that of GR. Triangles and solid lines are the relative difference for $\delta_0 = \pm 0.5$; squares and dotted lines, for $\delta_0 = \pm 0.35$.

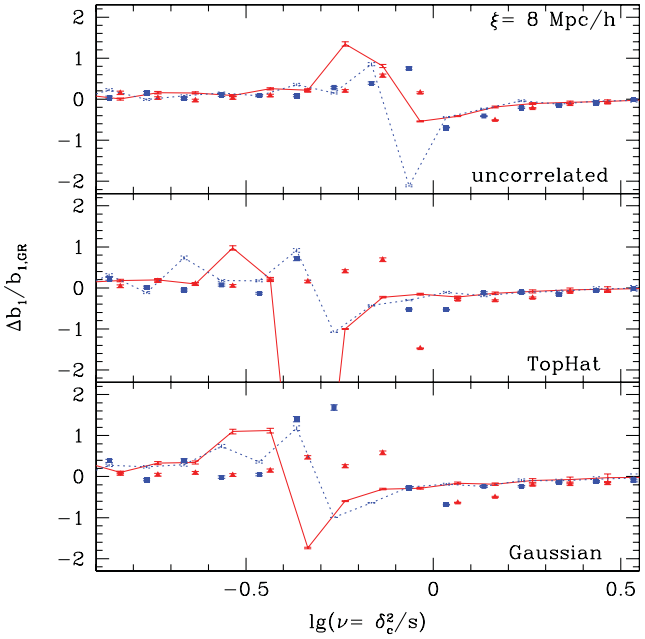

Figure 13. Relative difference in halo bias for chameleon models (Lagrangian environment) from that of GR.

$\delta_0 = \pm 0.35$). Combining the measurements of the halo bias in very overdense and underdense environments with the GR predictions (analytical formula or measurements from numerical simulations) would probably constrain the chameleon models.

5 CONCLUSIONS

In this paper we investigated the modifications in the mass function and the halo bias arising from the fifth force in the framework of the excursion set approach. Two environment definitions (Eulerian environment at $\zeta = 5\,\mathrm{Mpc}\,h^{-1}$ and Lagrangian environment at $\xi = 8\mathrm{Mpc}\,h^{-1}$) are combined with three smoothing window functions: Gaussian, tophat and sharp-k, to study how correlations between different scales induced by the window functions interact with the fifth force.

The halo formation barrier in the chameleon model depends on the environment density $\delta_{\rm env}$ – in a companion paper (Li & Lam 2012), we discuss the change in the mass function for a Eulerian environment versus Lagrangian environment for uncorrelated steps (i.e. sharp-k window filter) using the excursion set approach. In that case, the difference in the two environments only modifies the distribution of $\delta_{\rm env}$ and subsequently the first-crossing distribution. An additional effect owing to the non-trivial correlations between different smoothing scales arises when the smoothing function is Gaussian or tophat. We used Monte Carlo simulations to demonstrate that the additional correlations indeed modify the first-crossing distribution and the contribution is significant, particularly in the intermediate- to low-mass range. We then applied the analytical formalism proposed in Musso & Sheth (2012) to compute the first-crossing distribution for correlated steps. The analytical prediction matches the Monte Carlo simulations well for the high-mass regime. Having shown the significance of correlated steps in the unconditional first-crossing distribution, we examined the conditional mass function in chameleon models. When the steps in the excursion set are uncorrelated, the condition that random walks have passed through some δ_0 at a prescribed large scale S_0 only alters the distribution of $\delta_{\rm env}$ owing to the Markovian nature of uncorrelated steps. Correlated steps (the random walk is non-Markovian) introduce an additional effect owing to the non-trivial correlations between S_0 and all other scales. We compared the change in the first-crossing distribution owing to the fifth force for conditional walks with that for unconditional walks and found that walks in underdense large-scale environments experience a stronger modification than those in overdense large-scale environments – this effect is observed for all three smoothing window functions (with different strengths) usually used in the literature. Hence combining the conditional halo mass function in underdense large-scale environments with the unconditional mass function can potentially provide a strong probe for modified gravity.

Finally, we investigated how the chameleon models modify the halo bias derived from the excursion set approach. We found that the fifth force can modify the halo bias by a factor of a few for intermediate- to low-mass halos when an underdense large-scale environment is assumed. In addition, we found that, when correlated steps are used, the masses at which the halo bias is modified by the chameleon-type fifth force can be quite different for overdense and underdense environments. While this difference depends on the value of δ_0, we found that $\Delta \lg(\nu) = 0.4$ when δ_0 at the 2-σ level for $S_0 = 0.15^2\delta_{c0}$.

The effect of the correlations between different smoothing scales introduced by the use of different smoothing window functions on halo abundance and halo bias has been the focus of various recent studies. Its application with the excursion set approach in the chameleon models results in further modifications in both halo abundance and halo bias. In particular, the changes in the conditional mass function and the halo bias in underdense environments may provide potentially strong constraints on the chameleon models. We are also investigating the strength of correlations between the halo formation and the surrounding environment by measuring halo abundance and clustering under different environments in numerical simulations of chameleon models. This will be left for a future paper.

ACKNOWLEDGMENTS

TYL would like to thank Ravi Sheth for discussions. TYL is supported in part by a Grant-in-Aid for Young Scientists (22740149) and by WPI Initiative, MEXT, Japan. BL is supported by the Royal Astronomical Society and the Department of Physics of Durham University, and acknowledges the hospitality of Kavli-IPMU, where this work was initiated.

REFERENCES

Bernardeau F., 1994, ApJ, 427, 51
Bond J. R., Cole S., Efstathiou G., Kaiser N., 1991, ApJ, 379, 440
Brax P., van de Bruck C., Davis A. C., Shaw D. J., 2008, Phys. Rev. D, 78, 104021
Brax P., van de Bruck C., Davis A. C., Shaw D. J., 2010, Phys. Rev. D, 82, 063519
Brax P., Rosenfeld R., Steer D. A., 2010, JCAP, 08, 033
Brax P., van de Bruck C., Davis A. C., Li B., Shaw D. J., 2011, Phys. Rev. D, 84, 123524
Clifton T., Ferreira P. G., Padilla A., Skordis C., 2012, PhR, 513, 1
Davis A. C., Li B., Mota D. F., Winther H. A., 2012, ApJ, 748, 61
Hinterbichler K., Khoury J., 2010, Phys. Rev. Lett., 104, 231301
Hu W., Sawicki I., 2007, Phys. Rev. D, 76, 064004
Jain B., Khoury J., 2010, Ann. Phys., 325, 1479
Khoury J., Weltman A., 2004, Phys. Rev. D, 69, 044026
Lam T. Y., Sheth R. K., 2009, MNRAS, 398, 2143
Li B., 2011, MNRAS, 411, 2615
Li B., Barrow J. D., 2007, Phys. Rev. D, 75, 084010
Li B., Barrow J. D., 2011, Phys. Rev. D, 83, 024007
Li B., Efstathiou G., 2012, MNRAS, 421, 1431
Li B., Lam T. Y., 2012, MNRAS, 425, 730
Li B., Zhao H., 2009, Phys. Rev. D, 80, 044027
Li B., Zhao H., 2010, Phys. Rev. D, 81, 104047
Li B., Zhao G., Teyssier R., Koyama K., 2012a, J. Cosmol. Astropart. Phys., 1, 51
Li B., Zhao G.-B., Koyama K., 2012b, MNRAS, 421, 3481
Ma C., Maggiore M., Riotto A., Zhang J., 2011, MNRAS, 411, 2644
Maggiore M., Riotto A., 2010, ApJ, 711, 907
Mo H. J., White S. D. M., 1996, MNRAS, 282, 347
Mota D. F., Shaw D. J., 2007, Phys. Rev. D, 75, 063501
Musso M., Sheth R. K., 2012, MNRAS, 423, 102
Oyaizu H., 2008, Phys. Rev. D, 78, 123523
Oyaizu H., Lima M., Hu W., 2008, Phys. Rev. D, 78, 123524
Paranjape A., Sheth R. K., 2012, MNRAS, 419, 132
Paranjape A., Lam T. Y., Sheth R. K., 2012a, MNRAS, 420, 1429
Paranjape A., Lam T. Y., Sheth R. K., 2012b, MNRAS, 420, 1648
Schmidt F., Lima M., Oyaizu H., Hu W., 2009, Phys. Rev. D, 79, 083518
Sheth R. K., 1998, MNRAS, 300, 1057
Sheth R. K., Tormen G., 1999, MNRAS, 308, 119
Zhang J., Hui L., 2006, ApJ, 641, 641
Zhao G., Li B., Koyama K., 2011, Phys. Rev. D, 83, 044007

This paper has been typeset from a TEX/LATEX file prepared by the author.